Electronic supplementary information

Ternary TiO_2/SiO_x@C nanocomposite derived from a novel titanium-silicon MOF for high-capacity and stable lithium storage

Wenchao Shi, Jiashen Meng, Qi Li, Zhitong Xiao, Xiaoming Xu, Mingsheng Qin, Xiao Zhang and Liqiang Mai*

State Key Laboratory of Advanced Technology for Materials Synthesis and Processing, Wuhan University of Technology, Wuhan 430070, China

Email: qi.li@whut.edu.cn

Experimental

Synthesis of TiO_2/SiO_x@C nanocomposite

The porous TiO_2/SiO_x@C nanocomposite was prepared by a simple two-step process. Firstly, the precursor, namely Ti-Si MOF, was synthesized through solvothermal method [1]. 2 g of p-phthalic acid were added into a mixed solution of 36 mL DMF and 4 mL methanol, stirred for 20 min, followed adding titanium tetrabutoxide (TBOT) and tetraethyl orthosilicate (TEOS), according to the mole ratio of TBOT/TEOS=9:1, 8:2, 7:3, 6:4, 5:5, respectively, and the mole ratio of (TBOT+TEOS)/PTA=1:4. After stirring 20 min, the solution was transferred into a Teflon-sealed autoclave and kept at 160 °C for 24 h. The Ti-Si MOF was collected by centrifugation, washed with DMF for 3 times and methanol for 3 times and dried. To obtain TiO_2/SiO_x@C, the Ti-Si MOF was aged at 700 °C for 4 h in N_2 with a speed 5 °C min^{-1}. For comparison, MIL-125 (Ti) and TiO_2@C were prepared according to the abovementioned method just adding 1.04 mL TBOT but not TEOS.

Characterization

The structures of the materials were characterized on a D8 Advance X-ray diffractometer with Cu Kα radiation (λ=1.5406 Å). Field-emission scanning electron microscopy (FESEM) images of the samples was conducted via a

JEOL-7100F scanning electron microscope. Transmission electron microscopy (TEM) images and energy dispersive X-ray spectra (EDX) elemental mappings were collected on a JEM-2100F microscope. The BET surface areas and pore volumes were determined based on a Tristar-3020 instrument at 77 K. Raman spectra and Fourier transform infrared (FT-IR) spectra were recorded by the micro-Raman spectroscopy system (Renishaw INVIA). The carbon contents were obtained from thermos-gravimetric (TG) (NETZSCH STA 449F5) measurements, during which the samples were heated to 800 $^{\circ}$C in air with a heating rate of 10 $^{\circ}$C min^{-1}. X-ray photoelectron spectroscopy (XPS) results were collected by a VG MultiLab 2000 instrument.

The electrochemical performance of the synthesized TiO_2/SiO_x@C nanocomposite was evaluated using coin-type cells (CR2016) with lithium metal as the counter electrode. The working electrodes were composed of the active materials, acetylene black and carboxymethylcellulose at a mass ratio of 70:20:10 onto a copper foil. After dring at 70 $^{\circ}$C for 12 h, the electrode film was cut into circular discs of about 8 mm in diameter. The coin cells were assembled in an argon-filled glove box. The electrolyte used was composed of 1 M $LiPF_6$ in a mixture of ethylene carbonate (EC), diethyl-carbonate (DC), and dimethyl carbonate (DEC) (1:1:1 by volume). Cyclic voltammetry (CV) curves were tested on a CHI 600E electrochemical workstation between 0.01 to 3 V at a scan rate of 0.1 mV s^{-1}. The galvanostatic cycling tests were carried out in the voltage range of 0.01 – 3 V versus Li^+/Li with LAND CT2001A tester at different current densities. Electrochemical impedance spectroscopy (EIS) tests were performed on Autolab PGSTAT 302N in a frequency range of 0.01–100 kHz.

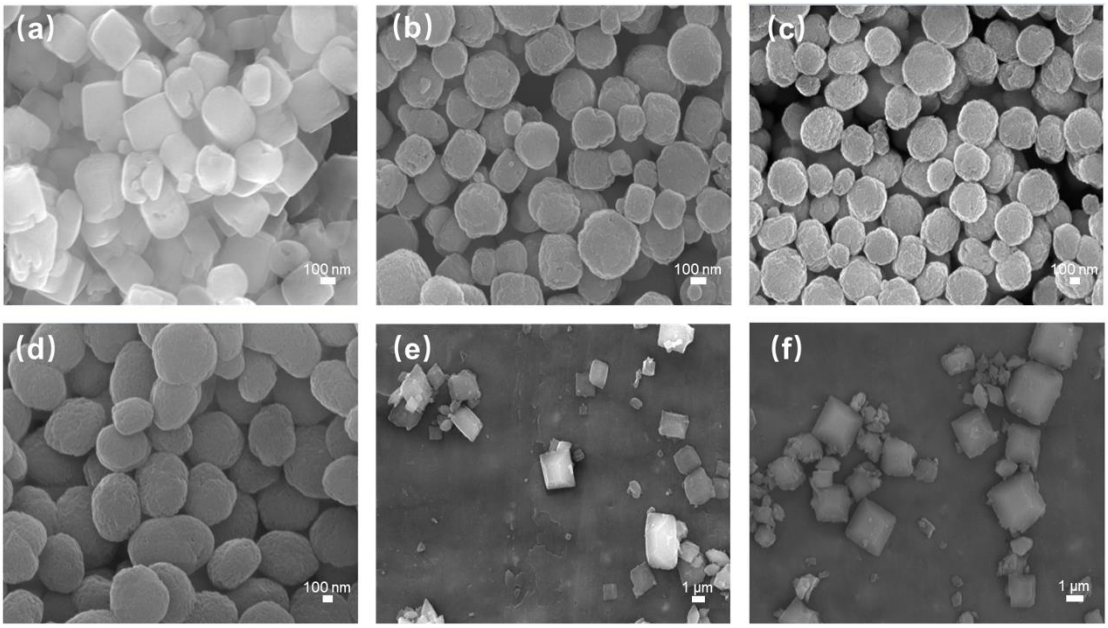

Fig. S1. SEM images of Ti-Si MOF of different feeding proportions of 10:0 (a), 9:1 (b), 8:2 (c), 7:3 (d), 6:4 (e), 5:5 (f).

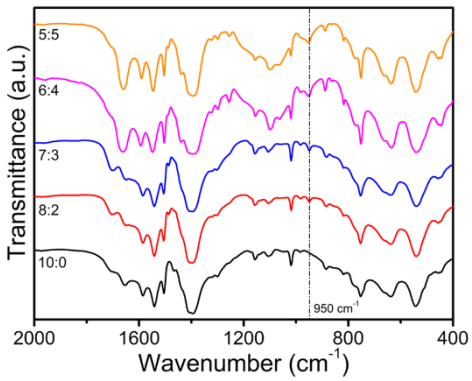

Fig. S2. FT-IR spectra of Ti-Si MOF precursors of different feeding proportions.

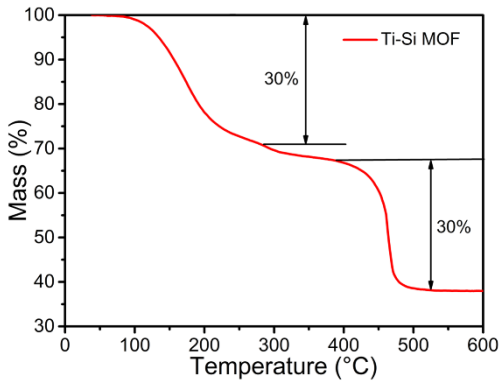

Fig. S3. TGA curve of the Ti-Si MOF precursor.

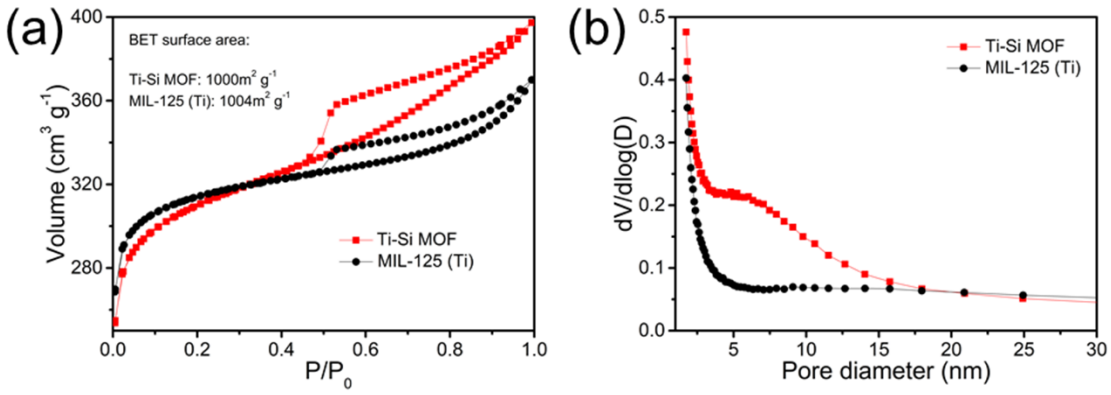

Fig. S4. Different samples of N_2 adsorption desorption isotherm (a) and corresponding pore size distribution (b).

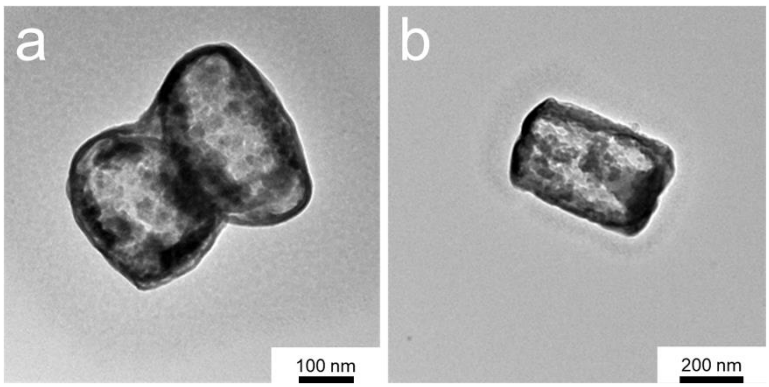

Fig. S5. The carbon matrix obtained by treatment with excess aqueous HF solution.

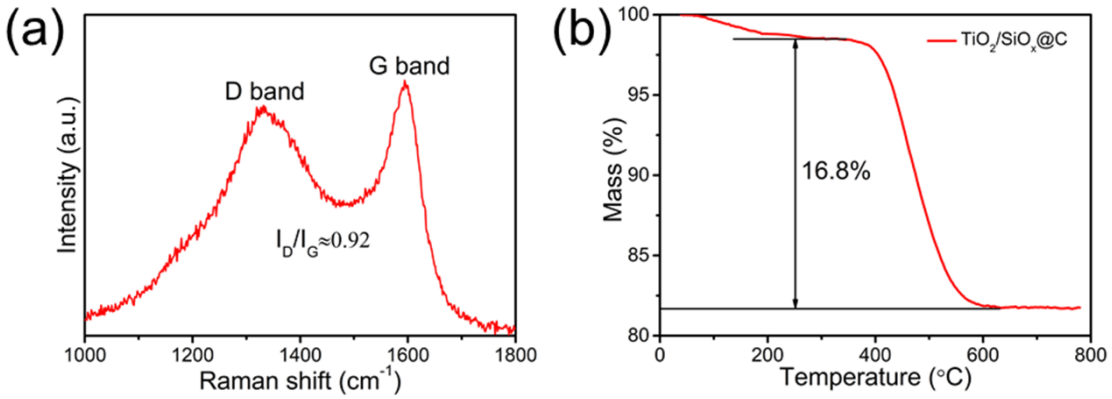

Fig. S6. Characterizations of TiO_2/SiO_x@C. (a) Raman spectrum. (b) TGA curve.

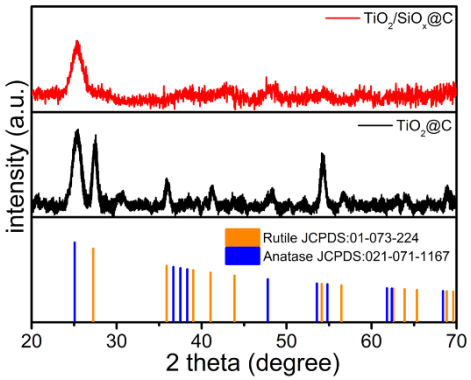

Fig. S7. XRD patterns of TiO_2/SiO_x@C and TiO_2@C.

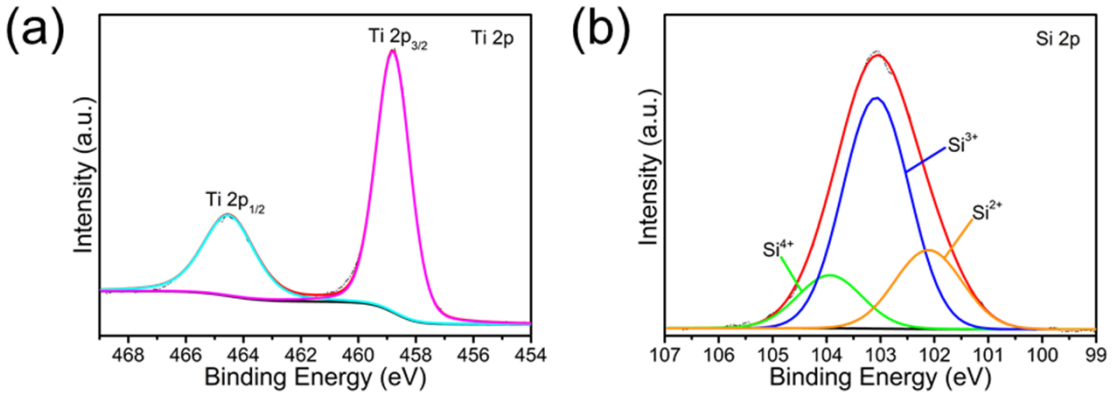

Fig. S8. XPS spectra of TiO_2/SiO_x@C. (a) Ti 2p. (b) Si 2p.

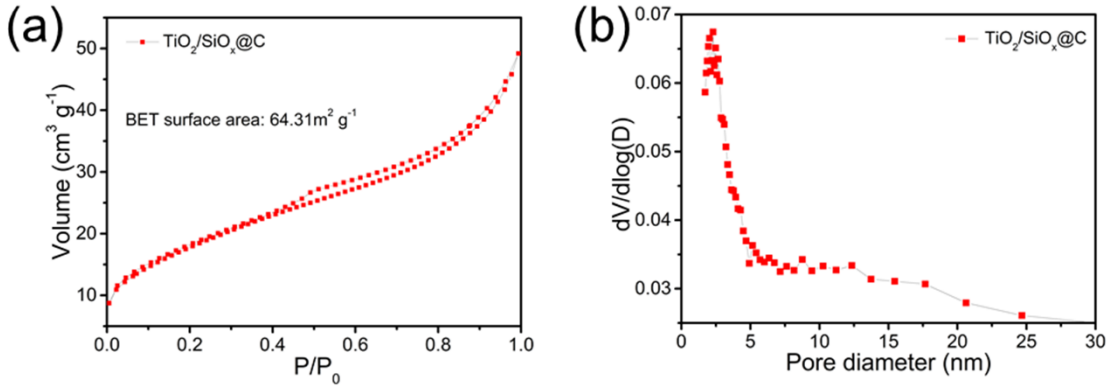

Fig. S9. N_2 adsorption/desorption isotherms TiO_2/SiO_x@C (a) and corresponding pore size distribution (b).

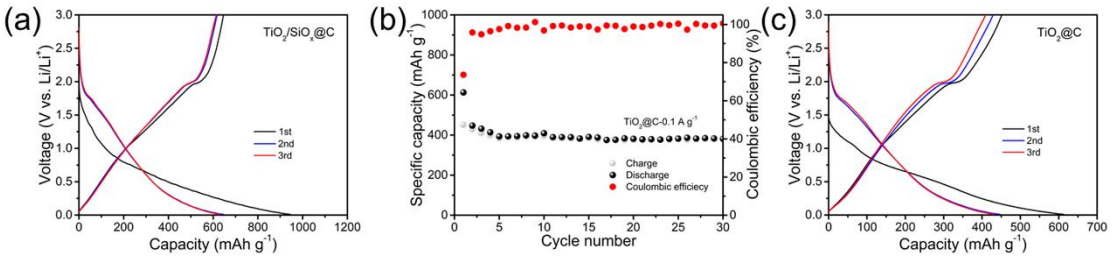

Fig. S10. The electrochemical performances of TiO_2/SiO_x@C and TiO_2@C electrodes. (a) The first three charge and discharge profiles of TiO_2/SiO_x@C at 0.1 A g^{-1}. (b) The performance of TiO_2@C at 0.1 A g^{-1} and corresponding first three charge and discharge profiles (c) of TiO_2@C.

The capacity contribution of SiO_x in the TiO_2/SiO_x@C was calculated through analyzing the reaction between SiO_x and Li. First, the reaction between SiO_x and Li follows the equations:[2]

(1)

$$2SiO_x + 3.75(2-x)Li \rightarrow (2-x)Li_{3.75}Si + xSiO_2$$

(2)

$$xSiO_2 + \frac{7.75x}{2}Li \rightarrow \frac{x}{2}Li_{3.75}Si + \frac{x}{2}Li_4SiO_4$$

The reactions of (1) and (2) are combined follow the following equation:

(3)

$$2SiO_x + \left(7.5 + \frac{x}{8}\right)Li \rightarrow \left(2 - \frac{x}{2}\right)Li_{3.75}Si + \frac{x}{2}Li_4SiO_4$$

Therefore, the theoretical first discharge capacity of $SiO_{1.465}$ is calculated to be ~ 2000 mAh g^{-1}. From Fig. 10a and Fig. 10c, the first discharge capacities of TiO_2/SiO_x@C and TiO_2@C are ~ 945 and ~ 613 mAh g^{-1}, while the first charge reversible capacities are ~ 647 and ~ 451 mAh g^{-1}. The Li-insertion ability of TiO_2 and carbon composite component in TiO_2/SiO_x@C is assumed similar to that of TiO_2@C. Then according to the mass fraction, the capacity of TiO_2 and carbon composite component in TiO_2/SiO_x@C at the first discharge process can be calculated to be (62.4% + 16.8%) × 613 mAh g^{-1} ≈ 485 mAh g^{-1}, the capacity of SiO_x component is (945 – 485) mAh g^{-1} = 460 mAh g^{-1}. From the actual delivered capacity and combining its mass fraction, the first discharge capacity of $SiO_{1.465}$ is calculated to be (460 ÷ 20.8%) mAh g^{-1} ≈ 2210 mAh g^{-1}. Therefore, the theoretical capacity calculated from the reaction equations is not much different from the first discharge capacity inferenced from the actual capacity. Therefore, this assumption and calculation method are reasonable. Further, the reversible capacity of $SiO_{1.465}$ can be calculated from equation (3) to be ~ 1240 mAh g^{-}

[1]. Thus, SiO_x in TiO_2/SiO_x@C provide reversible capacity of (1240 × 20.8%) mAh g^{-1} ≈ 260 mAh g^{-1}, while the TiO_2 and carbon composite component in TiO_2/SiO_x@C can provide reversible capacity of (647 – 260) mAh g^{-1} = 387 mAh g^{-1}.

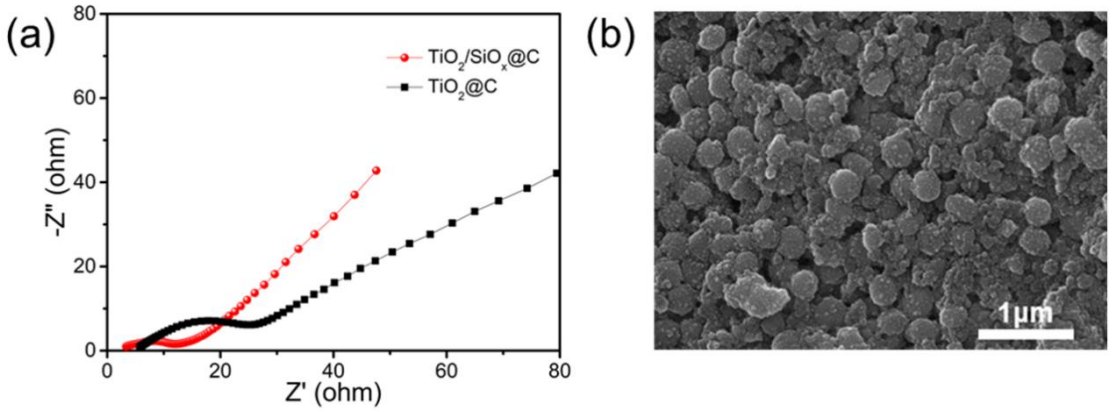

Fig. S11. Characterizations of different electrodes at 1 A g^{-1} after 100 cycles. (a) EIS profiles of TiO_2/SiO_x@C and TiO_2@C electrodes. (b) SEM image of TiO_2/SiO_x@C electrode.

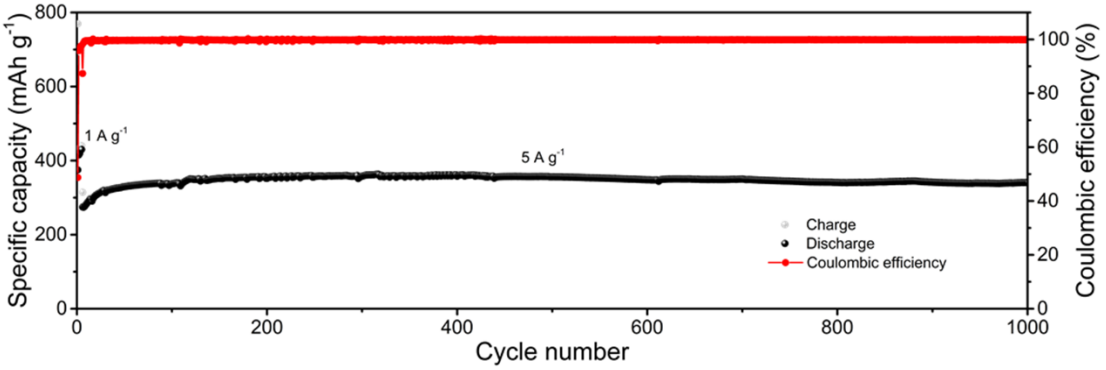

Fig. S12. Long cycle performance of TiO_2/SiO_x@C at the current density of 5 A g^{-1}.

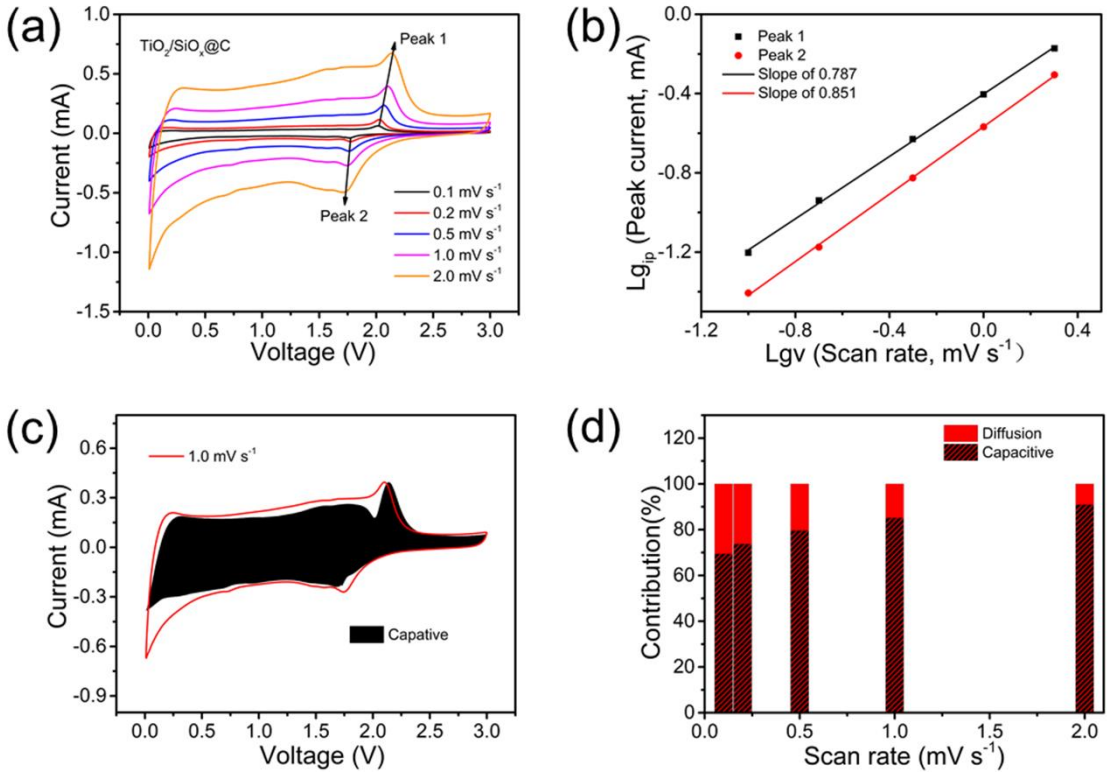

Fig. S13. Characterizations and analyses of electrochemical kinetics of TiO_2/SiO_x@C. CV curves (a) of the TiO_2/SiO_x@C at different scan rates and corresponding b values (b)for different peaks. (c) The separation of the capacitive and diffusion currents in TiO_2/SiO_x@C at a scan rate of 1 mV s^{-1}. (d) The percentage of capacitive contribution at different scan rates.

It is generally believed that the peak currents (i_p) and scan rates (v) in the CV tests follow the formula: $i_p = av^b (or\ lgi_p = lga + blgv)$, where a is a constant and b is considered to be the slope of the fitting line. When b value approaches 0.5, it represents the diffusion-controlled lithium storage process, while when b value approaches 1.0, it represents the capacitive-controlled process[3]. CV curves of the TiO_2/SiO_x@C electrode at various scan rates were investigated (Fig. S13a). The b values of TiO_2/SiO_x@C at the chosen two peaks confirm that the pseudo-capacitance contribution (Fig. S13b). The capacitive attribution was assessed to be ~ 85% at a scan rate of 1 mV s^{-1} as exhibited in shadow region (Fig. S13c). Moreover, the capacitive contribution of TiO_2/SiO_x@C increased with scan rates increasing (Fig. S13d).

Table. S1. Molar ratios of elements in the obtained TiO_2/SiO_x@C material.

Element	Norm. at.%
C	**36.89235**
O	**38.11405**
Si	**4.666116**
Ti	**20.32748**

Table. S2. Electrochemical performances of various TiO_2-based anodes for LIBs.

Materials	Voltage window	Specific capacity (mAh/ g^{-1})/Current density (A g^{-1})/Cycle number	Rate capacity (mAh g^{-1}) Current density (A g^{-1})	Ref.
TiO_2/SiO_x@C nanocomposite	**0.01-3 V**	**586/0.1/100**	**401/5**	**This work**
Rutile TiO_2/C	0-3.0 V	400/0.1/100	172/5	4
Anatase TiO_2/C	0.01-3 V	~180/0.08/100	123/0.8	5
Anatase TiO_2/RGO	1.0-3.0 V	174/0.17/200	88/3.4	6
TiO_2(B)/C	0.01-3.0 V	560/0.03/100	200/0.75	7
TiO_2-C/MnO_2	0.01-3 V	352/0.335/100	235/3.35	8
C/SiO_x/TiO_2	0.01-3 V	400/0.0668/100	200/1.67	9
TiO_2/SiO_x/C	0.005 – 3 V	421/0.067/100	---	10
SiO@TiO_2	0.1 – 3 V	901/0.2/200	272/3	11
TiO_2-C-SiO	0.005 – 2 V	674.5/0.14/100	800/1.4	12
TiO_2/SiO_2-C	0.0 – 3.0 V	502/0.1/300	232/2	13

Reference

1. Y. Fu, D. Sun, Y. Chen, R. Huang, Z. Ding, X. Fu and Z. Li, *Angew. Chem.-Int. Edit.*, 2012, **51**, 3364-3367.
2. M. Yamada, A. Inaba, A. Ueda, K. Matsumoto, T. Iwasaki and T. Ohzuku, *J. Electrochem. Soc.*, 2012, **159**, A1630-A1635.
3. V. Augustyn, J. Come, M. A. Lowe, J. W. Kim, P. L. Taberna, S. H. Tolbert, H. D. Abruna, P. Simon and B. Dunn, *Nat. Mater.*, 2013, **12**, 518-522.
4. P. Wang, J. Lang, D. Liu and X. Yan, *Chem. Commun.*, 2015, **51**, 11370-11373.
5. C. Zhang, Q. Zhang, S. Kang and X. Li, *J. Mater. Chem. A*, 2014, **2**, 2801-2806.
6. Z. Wang, J. Sha, E. Liu, C. He, C. Shi, J. Li and N. Zhao, *J. Mater. Chem. A*, 2014, **2**, 8893-8901.
7. Z. Yang, G. Du, Z. Guo, X. Yu, Z. Chen, T. Guo and H. Liu, *J. Mater. Chem.*, 2011, **21**, 8591-8596.
8. J. Y. Liao, D. Higgins, G. Lui, V. Chabot, X. Xiao and Z. Chen, *Nano Lett.*, 2013, **13**, 5467-5473.
9. Z. Yang, Y. Ding, Y. Jiang, P. Zhang and H. Jin, *Nanotechnology*, 2018, **29**, 405602.
10. X. Wang, Y. Xia, X. Zuo, S. J. Schaper, S. Yin, Q. Ji, S. Liang, Z. Yang, S. Xia and Y. Xiao, *Ceram. Int.*, 2019, **45**, 14327-14337.

11. D. Xu, W. Chen, Y. Luo, H. Wei, C. Yang, X. Cai, Y. Fang and X. Yu, *Appl. Surf. Sci.*, 2019, **479**, 980-988.
12. F. Dou, L. Shi, P. Song, G. Chen, J. An, H. Liu and D. Zhang, *Chem. Eng. J.*, 2018, **338**, 488-495.
13. W. Liu, T. Yao, S. Xie, Y. She and H. Wang, *Nanomaterials*, 2019, **9**, 68.